Magnitude-Based Angle-of-Arrival Estimation, Localization, and Target Tracking

Chitra R. Karanam*
University of California Santa Barbara
Santa Barbara, California
ckaranam@ece.ucsb.edu

Belal Korany*
University of California Santa Barbara
Santa Barbara, California
belalkorany@ece.ucsb.edu

Yasamin Mostofi
University of California Santa Barbara
Santa Barbara, California
ymostofi@ece.ucsb.edu

ABSTRACT

In this paper, we are interested in estimating the angle of arrival (AoA) of all the signal paths arriving at a receiver array using only the corresponding received signal magnitude measurements (or, equivalently, the received power measurements). Typical AoA estimation techniques require phase information, which is not available in some WiFi/Bluetooth receivers, and is further challenging to properly measure in a synthetic antenna array due to synchronization issues. In this paper, we then show that *AoA estimation is possible with only the received signal magnitude measurements.* More specifically, we first propose a framework, based on the spatial correlation of the received signal magnitude, to estimate the AoA of signal paths from fixed signal sources (both active transmitters and passive objects). Next, we extend our AoA estimation framework to a dual setting, and further utilize a particle filter, to show how a moving target (both active transmitters and passive robots/humans) can be tracked, based on only the received signal magnitude measurements of a small number of fixed receivers. We extensively validate our proposed framework with several experiments (total of 22), in both closed and open areas. More specifically, we first utilize a robot to emulate an antenna array, and estimate the AoA of active transmitters, as well as passive objects using only the received WiFi signal magnitude measurements. We next validate our tracking framework by using only three off-the-shelf WiFi devices as receivers, to track an active transmitter, a passive robot that writes the letters of IPSN on its path, and a walking human. Overall, our results show that AoA can be estimated, with a high accuracy, with only the received signal magnitude measurements, and can be utilized for high quality angular localization and tracking.

CCS CONCEPTS

• **Hardware** → **Sensor applications and deployments**; **Wireless devices**; • **Computer systems organization** → *Sensor networks*; *Robotics*;

*Co-first authors

KEYWORDS

Angle-of-arrival, Localization, Tracking, WiFi, Magnitude-based AoA estimation

1 INTRODUCTION

In recent years, there has been an increasing interest in using Radio Frequency (RF) signals to obtain information about our surroundings. Imaging, localization, tracking, occupancy estimation, and human activity recognition are some of the many RF sensing applications [3, 5–9, 14, 19, 30]. Localization and tracking, in particular, are crucial techniques that can be useful in many scenarios such as emergency response, radio navigation, security, surveillance, and smart homes. Angle of Arrival (AoA) estimation, on the other hand, is an important problem that can be used towards localization and tracking. However, most AoA estimation approaches require synchronized phase information, which can not be obtained on a synthesized array of off-the-shelf RF transceivers.

In this paper, we show how to estimate the AoA of the signal paths arriving at a receiver array, only from the received signal magnitude measurements (or, equivalently, the received power measurements). We then propose a unified framework for angular localization of fixed passive/active objects, as well as tracking of passive/active targets, using our magnitude-only AoA estimation foundation.

AoA estimation is a classical problem that has gained a considerable attention in the field of array signal processing. Many solutions have been proposed in the literature, including traditional beamforming [28], MUSIC [24], and ESPRIT [23]. All of these techniques assume that the received signal phase measurements are available and synchronized across the elements of a measurement array. However, many of the commercial off-the-shelf (COTS) wireless devices do not provide stable absolute phase measurements [33], making the synthesis of a long array not possible due to synchronization issues. There have been attempts to stabilize the phase measurements in COTS devices (e.g., Intel 5300 WLAN card), but these approaches do not result in synchronized phase measurements required for array signal processing [33]. Few works have investigated the problem of AoA estimation using only the signal power (or equivalently, magnitude) measurements at the array elements. For instance, in [18], mechanical steering of a directional antenna is utilized, whereas in [21], special type of antennas that have multiple radiation patterns are used. Such work, however, require custom-made hardware. As for array processing techniques using magnitude-only measurements, [15] proposes a sparsity-based optimization problem which assumes the knowledge of the number of sources, and [26] proposes an algorithm that can only find a function of the differences between the AoAs, but not the AoAs themselves. Furthermore, the

DOI 10.1109/IPSN.2018.00053

aforementioned papers are only validated in a simulation environment, and with only active transmitters. In this paper, we propose and experimentally validate a framework for estimating the AoAs of active transmitters as well as passive objects, using only the received signal magnitude.

We then adapt and extend our proposed AoA estimation framework for tracking a passive/active moving target, using only a small number of receivers. Target tracking has been of interest to the research community in the past few years. Some existing tracking work relies on signals with a large bandwidth [4], while others rely on the availability of a stable absolute phase measurement by using a software defined radio to track [32], or to estimate the direction of motion [1]. However, large bandwidths or stable absolute phase information are not available in COTS devices. There are a number of works that have demonstrated tracking using COTS devices, albeit with a different approach than ours. However, most of these require several transceivers, and/or require extensive prior calibration experiments in the same environment, and/or are computationally very expensive. For instance, [31] depends on fingerprinting the target location and comparing the actual tracking data to the fingerprint database, which requires extensive prior calibration and training. In [3], the target is tracked using the RSSI measurements, and a link crossing model, but it requires a dense sensor deployment all around the area (e.g., 30 transceivers). While the number of sensors is reduced in [17, 22], they still require 6 links and a very high computational complexity. [29], on the other hand, needs extensive prior measurements in the same area.

Contribution Statements: In this paper, we propose a unified framework that can be used towards angular localization of fixed active or passive objects, as well as tracking of a moving active or passive target, using only the magnitude of the received signal at a small number of receivers. Our framework has a very small computation time, does not require any prior calibration in the same environment, and has a good tracking and localization quality. More specifically,

- We propose an approach to estimate the AoA of signal paths arriving at a receiver array using only the magnitude of the corresponding received measurements. Our approach shows that the auto-correlation function (and therefore the power spectrum) of the received signal magnitude at the receiver array carries vital information on the AoA, an analysis which will then be the foundation for our proposed methodologies throughout the paper. For instance, we propose a framework for the case of angular localization of fixed active transmitters or passive objects/humans, based on this foundation.
- We extend our proposed AoA estimation framework to a dual setting for tracking a moving target. Our proposed framework utilizes only the magnitude of the received signal at a small number of receivers, and further utilizes particle filters and motion dynamics. Our approach can track active transmitting targets as well as passive moving objects or humans.
- We validate both our angular localization framework and tracking approach with extensive experiments (total of 22) in various closed and open areas and show that our approach can achieve high-quality localization and tracking. More specifically, we first utilize a robot to emulate an antenna array and estimate the AoA of active transmitters and passive objects, using only WiFi magnitude measurements. Our angular localization has an overall Mean Absolute Error (MAE) of 2.44°, and only takes an average of 0.45 seconds to localize up to four sources/objects. We next validate our tracking framework by using only three off-the-shelf WiFi devices as receivers, and track an active transmitter, a passive robot that writes the letters of *IPSN* on its path, and a walking passive human. Our tracking approach can achieve an MAE of 20 cm for active targets and 26.75 cm for passive ones, and only takes an average of 1.05 seconds to run per 1 m of tracking length. Overall, our results show that AoA can be estimated, with a high accuracy, with only the received signal magnitude measurements, and can be used for efficient angular localization and tracking.

We note that if phase can be more reliably synchronized in a synthesized array of COTS receivers in future, then our approach can provide an additional sensing mechanism for AoA estimation, and can thus result in a considerably better overall estimation quality using both magnitude and phase. The rest of this paper is organized as follows. In Sec. 2, we show our problem formulation for a general setting of signal paths arriving at an array. In Sec. 3, we propose a framework for AoA estimation of signals arriving from fixed sources, and the corresponding angular localization of objects, and show its performance through extensive experiments. In Sec. 4, we adapt our framework to track a moving target. We experimentally validate our proposed approach for tracking active and passive moving targets, including humans and robots. Finally, we present a discussion on the limitations and future extensions of our proposed approach in Sec. 5, and conclude in Sec. 6.

2 OUR AOA ESTIMATION FOUNDATION

Consider N signal paths arriving at a linear receiver array at various angles, as shown in Fig. 1. These signal paths can be caused by active transmitting sources or by passive objects that got illuminated through a transmission in the area. We are then interested in estimating the AoA of these paths, corresponding to all the N sources/objects, using only the magnitude of the received signal at each antenna of the receiver array.[1] Note that for the case of passive objects, AoA estimation results in the angular localization of the objects. In this section, we show that the magnitude of the received signal at the array contains information about the AoA of all the signal paths. This foundation will then be the base for our proposed framework of Sec. 3 to estimate the AoA of all the sources, as well as for our proposed tracking approach of Sec. 4.

Consider the receiver array of Fig. 1. Let d denote the distance from the first antenna, as denoted on the figure. The baseband received signal, due to the N arriving paths, can be written as a function of distance d as follows [13],

$$c(d) = \sum_{n=1}^{N} \alpha_n e^{j\left(\mu_n - \frac{2\pi}{\lambda} d \cos(\phi_n)\right)} + \eta(d), \qquad (1)$$

where α_n is the amplitude of the n^{th} signal path, λ is the wavelength of the signal, ϕ_n is the AoA of the n^{th} path (measured with respect to the x-axis), μ_n is the phase of the n^{th} signal at the first antenna of the

[1]We use the term "source" for both active transmitters and passive objects in this paper.

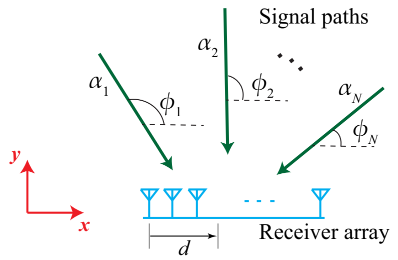

Figure 1: N Signal paths arriving at a receiver array.

array, and $\eta(d)$ is the receiver noise. Let $A_{\text{corr}}(\Delta)$ denote the auto-correlation function of the baseband received signal magnitude, $|c(d)|$, at lag Δ.

Lemma 2.1. *$A_{corr}(\Delta)$ can be written as follows [13],*

$$A_{corr}(\Delta) = C_A + C_{\sigma_\eta}\delta(\Delta) + \sum_{n=1}^{N-1}\sum_{m=n+1}^{N} C_{m,n}\cos\left(2\pi\frac{\Delta}{\lambda}(\psi_n - \psi_m)\right), \tag{2}$$

where C_A is a constant that depends on the total signal power, C_{σ_η} is a constant that depends on the noise variance σ_η^2 and the signal power, $C_{m,n} = \frac{\pi\overline{\alpha_m^2\alpha_n^2}}{16P}$, $\psi_n = \cos(\phi_n)$, $P = \sum_{n=1}^{N}\alpha_n^2$ is the total power of the received signal, and $\delta(.)$ is the Dirac Delta function.

Proof. See Appendix A. □

Then, by taking the Fourier transform of $A_{\text{corr}}(\Delta)$, we get,

$$\mathcal{A}(f) = C_A\delta(f) + C_{\sigma_\eta} + \sum_{n=1}^{N-1}\sum_{m=n+1}^{N}\frac{C_{m,n}}{2}\left(\delta[f - \frac{\psi_n - \psi_m}{\lambda}] + \delta[f + \frac{\psi_n - \psi_m}{\lambda}]\right). \tag{3}$$

Eq. 3 shows that $|\mathcal{A}(f)|$ has peaks at the frequencies $\pm(|\psi_n - \psi_m|)/\lambda$, for $1 \leq n < m \leq N$.[2] For the sake of simplicity, we normalize the frequency with respect to $\frac{1}{\lambda}$, so that the peaks in the spectrum occur at $\pm|\psi_n - \psi_m|, 1 \leq n < m \leq N$. It can be seen from Eq. 3 that the locations of the peaks of $|\mathcal{A}(f)|$ contain information about the AoA of the N signal paths. In the next section, we then propose a framework to use this information and estimate all the AoAs.

3 AOA ESTIMATION FOR FIXED SOURCES/OBJECTS

In this section, we consider the scenario where there are unknown fixed active or passive signal sources located in an area. We are then interested in estimating the AoAs of the signals from these sources at the receiver array, thus localizing the direction of these sources/objects, using only the magnitude of the corresponding received signal measurements. The signal measurements can be obtained by using an array of fixed antennas, or by using an unmanned vehicle that utilizes its motion to collect measurements along a route, thus synthesizing an antenna array. We next propose a framework to estimate the AoAs of signals from fixed sources. We present extensive experimental results for estimating the AoAs for both active and passive cases.

3.1 AoA Estimation Methodology

Consider N signal sources present on one side of a receiver array, i.e., sources whose AoAs $\{\phi_n, 1 \leq n \leq N\}$ satisfy $0° \leq \phi_n < 180°$ (see Fig. 1). Let $\Psi = \{\psi_1, \psi_2, \ldots, \psi_N\}$, where $\psi_n = \cos(\phi_n)$. Define the function $D(U)$ on a set of real numbers U as the set of all the unique pairwise distances between the elements of U, i.e. $D(U) = \{|u_i - u_j| : u_i, u_j \in U, i \neq j\}$. Let Q be the set of the absolute values of the pairwise differences of the cosines of AoAs, i.e. $Q = D(\Psi)$. Without loss of generality, we assume that Q is ordered: $Q = \{q_1, q_2, \ldots, q_M\}, q_1 > q_2 > \cdots > q_M$. We are then interested in estimating Ψ, and hence the AoAs, using the set of pairwise distances Q, obtained using Eq. 3.

The problem of estimating a set of N real numbers, B, given the multiset of absolute differences (distances) between every pair of numbers, ΔB, is called the Turnpike problem [16]. This problem has been explored extensively in the literature and solvers have been proposed for finding its solution [16]. However, it is not possible to obtain a unique solution set using just the set ΔB. For instance, for a solution B, the sets obtained through translation $B + \{e\} = \{b + e : b \in B\}$, mirroring $-B = \{-b : b \in B\}$, or a combination of both $-B + \{e\}$, would also result in the same set of distances ΔB, for any constant e. Furthermore, when the number of points $N \geq 6$, there exist other possible solutions that do not arise from the above construction [16].

The existing solvers for the Turnpike problem require that the set of distances should contain all the $\binom{N}{2}$ pairwise distances (or that we know the multiplicity of the non-distinct distances, if any), and they suffer from the translation and mirroring ambiguities as well as other ambiguities. In our AoA estimation problem though, we will not know the multiplicity of the possible non-distinct distances. Furthermore, we also have to resolve the aforementioned translation and mirroring ambiguity. Thus, we cannot utilize the solvers proposed for the Turnpike problem in our setting. Therefore, in this section we propose our approach to estimate the AoAs from the pairwise cosine distances.

In order to overcome the ambiguity arising due to the translation and mirroring of Ψ, we can place a reference signal source (i.e., a transmitter) at one extreme of the span of angles, say $\phi_{\text{ref}} = 0°$, so that $\psi_{\text{ref}} = 1$. This also implies that any valid solution set would only contain ψs that are less than or equal to ψ_{ref}, a condition we then utilize in our proposed methodology. However, there still exist multiple solutions for a set Q.

We next describe our proposed algorithm to first find all the valid sets of solutions $\{\psi_n : 1 \leq n \leq N\}$, for a given distance set Q. Then, we show how we can reduce the number of valid solutions (and possibly obtain a unique solution) by utilizing measurements from two arrays in different configurations.

3.1.1 *Proposed Approach for Finding All Possible Angle Solutions.*

We next describe how we can obtain all the valid solution

[2] Note that the Fourier transform of $|c(d)|^2$ also has a similar frequency content. However, the spectrum of $|c(d)|^2$ is considerably more noisy, as compared to $\mathcal{A}(f)$, since the effect of noise is minimized in the auto-correlation, due to the uncorrelated nature of the noise.

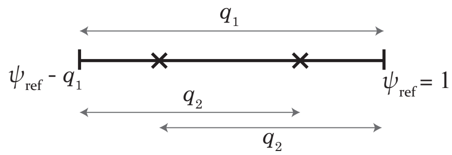

Figure 2: Illustration of the reference point, the positioning of the first point corresponding to q_1, and the two possible valid position choices for ψ_2, in our proposed approach.

sets corresponding to Ψ, given the ordered set of distances Q, the AoA corresponding to the reference source at $\phi_{\text{ref}} = 0°$, and the estimated number of sources (denoted by $\hat{N}$). We show how to estimate the number of sources in Sec. 3.1.2. Without loss of generality, we take the sets Ψ and Q to include the impact of the new added reference source at ϕ_{ref}, i.e., $\Psi = \{\psi_{\text{ref}}, \psi_1, \ldots, \psi_{N-1}\}$. Then, we are interested in estimating the angles of the rest $N-1$ unknown sources.

The rightmost and leftmost extreme points of the set Ψ are defined by $\psi_{\text{ref}} = 1$ and $\psi_1 = \psi_{\text{ref}} - q_1$, respectively, as shown in Fig. 2. Consider the positioning of the next point ψ_2, corresponding to q_2. Fig. 2 shows the two possible valid position choices for it. Both these will result in a valid solution set. Similarly, for each of the remaining distances $q_i, 3 \le i \le M$, there exist a pair of positions on the line in Fig. 2, whose distance to the two extreme points correspond to that q_i. It is easy to confirm that these two positions are the only possible positions given the monotonicity of the set Q. This observation is the base of our proposed approach, which we detail next. Let the set $\hat{\mathcal{S}}$ denote the set of all the sets of valid solutions. We start with a valid partial solution, where a Valid Partial Solution (VPS) is a set S such that $D(S) \subseteq Q$. We then find all the valid solutions, as follows:

Initialization: We initialize the set of VPSs with $\mathcal{S}^{(1)} = \{\{\psi_{\text{ref}} - q_1, \psi_{\text{ref}}\}\}$, which is the smallest VPS, containing only the two extreme points of Ψ.

Iteration Update: In iteration i, we place a point at a distance q_i from either of the extremes in the existing VPSs. More specifically, for each set $S \in \mathcal{S}^{(i-1)}$, we generate one test set by adding a point at a distance q_i from the rightmost extreme, and another test set by adding a point at a distance q_i from the leftmost extreme. If the pairwise distances of the new sets are a subset of Q, we then add these test sets to $\mathcal{S}^{(i-1)}$ to generate $\mathcal{S}^{(i)}$.

Algorithm Termination: The algorithm is terminated after $M-1$ iterations, which corresponds to exhausting all the elements of Q. A set $S \in \mathcal{S}^{(M)}$ is a possible solution for Ψ if the cardinality of S is $\hat{N}$ and $D(S) = Q$. We then use all such sets S to generate $\hat{\mathcal{S}}$, the final set of all the possible solutions. Algorithm 1 shows the pseudo-code for this algorithm.

Remark 1. *It can be easily confirmed that the aforementioned algorithm captures all the possible valid solution sets, even when there are distance multiplicities.*

Remark 2. *Note that ϕ_{ref} does not have to be necessarily $0°$. As long as it is the smallest possible angle (i.e., all the other angles are greater than it), then the previous algorithm works.*

While we have removed the ambiguity due to translation and mirroring, the previous algorithm can still result in a number of valid solutions. If there is no distance multiplicity, then we can prove that there will only be two solutions by using ψ_{ref}, when the number of unknown sources is less than 5 (see the Turnpike literature [16]). In general, however, there may be more than two possible solution sets. Next, we show how we can further reduce the number of possible solutions.

Algorithm 1 Finding all possible angle solutions

function findAllPossibleAngles(Q, ψ_{ref}, $\hat{N}$)
Initialize $\mathcal{S}^{(1)} \leftarrow \{\psi_{\text{ref}} - q_1, \psi_{\text{ref}}\}$
for all $2 \le i \le M$ **do**
    $\mathcal{S}^{(i)} \leftarrow \mathcal{S}^{(i-1)}$
    for all sets $S \in \mathcal{S}^{(i-1)}$ **do**
        $S_1^{\text{test}} \leftarrow S \cup \{\psi_{\text{ref}} - q_i\}$, and $S_2^{\text{test}} \leftarrow S \cup \{\psi_{\text{ref}} - q_1 + q_i\}$
        for all $k \in \{1, 2\}$ **do**
            if $D(S_k^{\text{test}}) \subseteq Q$ **then**
                $\mathcal{S}^{(i)} \leftarrow \mathcal{S}^{(i)} \cup S_k^{\text{test}}$
            end if
        end for
    end for
end for
$\hat{\mathcal{S}} \leftarrow \{S : S \in \mathcal{S}^{(M)}, \text{cardinality}(S) = \hat{N}, D(S) = Q\}$
return $\hat{\Phi}_{\text{all}} = \cos^{-1} \hat{\mathcal{S}}$

3.1.2 AoA Estimation with Multiple Routes. In order to reduce the ambiguity due to multiple possible solutions obtained using Algorithm 1, we propose to use another set of measurements collected by a receiver array with a different orientation. This new magnitude measurement can be obtained either by another fixed receiver array or by an unmanned vehicle that moves along a route with a different orientation. This solution is thus particularly suitable for the case of an unmanned vehicle emulating a receiver array, since traversing two straight routes is a trivial task for an unmanned vehicle. Fig. 3 shows an example of this scenario. Suppose that the AoAs of the signal sources for the first array configuration are $\{\phi_n : 1 \le n \le N\}$. For the second array that is tilted by an angle Ω in the clockwise direction, the AoAs are now $\{\phi_n + \Omega : 1 \le n \le N\}$ and the reference source has an angle of arrival Ω or equivalently, $\psi_{\text{ref}} = \cos(\Omega)$.

Since cosine is not a linear function of its argument, utilizing two sets of array measurements results in different sets of pairwise distances Q and Q'. Therefore, we can obtain the set of all possible angle solutions individually for Q and Q' (using Algorithm 1), and then take the intersection of the two sets to find the common valid solution(s). More specifically, let $\Phi_{\text{all},1}$ and $\Phi_{\text{all},2}$ indicate the AoA solution sets for Q and Q' respectively. The intersection of the two sets $\Phi_{\text{all},1}$ and $\Phi_{\text{all},2} - \{\Omega\}$ is then our final estimated AoAs.[3] Intuitively, the chance that the two routes have more than one possible common set is considerably small. However, it is challenging to theoretically prove the uniqueness, or derive the conditions

[3]Note that in practice, the angles from the two sets $\Phi_{\text{all},1}$ and $\Phi_{\text{all},2}$ (after subtracting Ω from $\Phi_{\text{all},2}$) may never be equal, owing to noise or rounding errors. Therefore, we need to compare the sets within a tolerance level.

for the uniqueness of the final solution set. Thus, we leave any such proof to future work. However, we have observed through extensive simulations for up to 8 signal sources that our algorithm results in a unique solution for the AoA estimation problem. Furthermore, if there is more than one solution set in the common set, we can collect measurements along another array route to obtain a unique solution. This online strategy is in particular suitable for the case of an unmanned vehicle emulating an array. We note that our proposed strategy is computationally very efficient. We report on sample times in the next section. We next discuss some aspects of the proposed approach.

Criteria for Choosing Ω*:* The orientation of the second array, Ω, determines the extent of dissimilarity between the sets Q and Q', where a larger Ω is likely to result in a higher dissimilarity. Therefore, it is preferable to use as large an Ω as possible. However, we require all the sources in the area to lie on one side of the receiver array (i.e., upper half plane) in the second configuration as well. Therefore, we can use the first set of distances Q, to estimate the largest AoA at the first receiver array as $\phi_{\max} = \cos^{-1}(1 - q_1)$. This implies that the possible range of values for Ω is $0 < \Omega < 180^\circ - \phi_{\max}$. Note that if ϕ_{ref} for the first route was $\phi_{\min} > 0$ instead of 0, where $\phi_{\min}$ is smaller than all source angles, then the condition for Ω becomes $-\phi_{\min} < \Omega < 180^\circ - \phi_{\max}$, where $\phi_{\max} = \cos^{-1}(\cos(\phi_{\min}) - q_1)$.

Choice of Number of Sources: Given a set of unique distances Q and Q', we are interested in estimating the AoAs corresponding to the smallest number of sources that can result in the two sets of distances. For N sources, the maximum number of possible pairwise distances is $\binom{N}{2}$. Suppose that the cardinality of sets Q and Q' are M and M'. Therefore, the estimated number of sources $\hat{N}$ should satisfy $M \le \binom{\hat{N}}{2}$ and $M' \le \binom{\hat{N}}{2}$, which translate to the conditions: $\hat{N} \ge \frac{1+\sqrt{1+8M}}{2}$ and $\hat{N} \ge \frac{1+\sqrt{1+8M'}}{2}$. Hence, we set $\hat{N}_{\min}$ as the smallest integer satisfying the previous two inequalities.

We start by assuming that we have $\hat{N} = \hat{N}_{\min}$ sources. We then solve for the AoAs for the sets Q and Q' separately, using the approach of Sec. 3.1 (Algorithm 1). If the intersection of $\Phi_{\text{all},1}$ and $\Phi_{\text{all},2} - \{\Omega\}$ is an empty set, we then need to increase $\hat{N}$ by 1, until we get a non-empty intersection set of solutions.

REMARK 3. *It is highly unlikely that adding an element* ψ_{new} *to the true set* $\mathbf{\Psi}$ *or taking out one element of it will produce the same* Q *and* Q' *respectively for both the routes. Hence, it is highly unlikely that using any* $\hat{N}$ *other than the true* N *will produce non-empty intersection set of solutions.*

REMARK 4. *For the case where we are interested in finding all the valid solutions with only one measurement array,* $\hat{N}$ *can be chosen as* $\hat{N}_{min} = \left\lceil \frac{1+\sqrt{1+8M}}{2} \right\rceil$*, which corresponds to the smallest number of sources that could have resulted in a cardinality of* M *for* Q*. If the current* $\hat{N}$ *does not result in a valid solution, we then keep increasing* $\hat{N}$ *by 1 until we get a non-empty solution set.*

3.1.3 Solution for the Special Case of Dominant Reference Source.

Consider the case that the signals from the unknown signal sources are of lower transmission power as compared to the reference source at ϕ_{ref}. *This case is in particular relevant when we are interested in estimating the direction of passive objects.* Then, the transmitted reference signal will bounce off of these objects and reach the receiver array with a considerably smaller power than that of the path from our reference transmitting source. In such a case, the AoA estimation problem is easier to solve, as we show next.

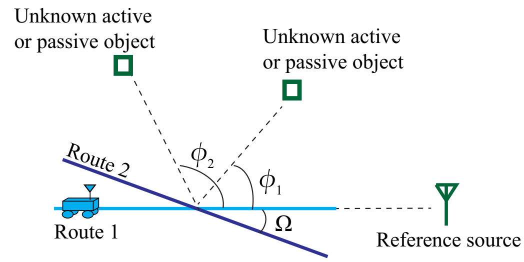

Figure 3: Framework for AoA estimation using two routes. Received signal magnitude measurements are collected along two arrays in order to reduce the ambiguity due to multiple sets of possible solutions to the AoA estimation problem.

Consider $N - 1$ unknown sources where the paths arriving from them at the receiver array have a lower power as compared to the reference source. This can happen for both the cases of active and passive sources. In the active case, this can happen when the active transmitters have a lower power as compared to our reference source. On the other hand, the passive case results in a dominant reference source almost all the time. Then, from Eq. 3, we can see that the pairwise coefficients $C_{m,n}$ that correspond to the reference source and an unknown source would be the only significant peaks in the spectrum. More specifically, if the dominant reference source with a higher power is at 0°, and the unknown sources are at angles $\{\phi_1, \ldots, \phi_{N-1}\}$, then the estimated differences from the spectrum are $Q = \{1-\cos(\phi_1), \ldots, 1-\cos(\phi_{N-1})\}$ since the rest of differences will have negligible peaks. Therefore, we can directly estimate the AoAs corresponding to the unknown sources as $\{\cos^{-1}(1 - q) : q \in Q\}$.

We next experimentally validate our proposed framework with several experiments for estimating the AoAs of both the active and passive signal sources.

3.2 Experimental Results for the Case of Fixed Sources/Objects

In this section, we present our experimental results and show the performance of our proposed framework for estimating the AoA in three scenarios: (a) fixed active (transmitting) sources, (b) fixed active sources with a dominant reference source, and (c) fixed passive objects. In the experiments, we use a TP-Link AC1750 WiFi router as a transmitter. The router operates in the 5 GHz band. The output signal of the router is split into N branches using a power divider, in order to create N signal sources for the fixed active source scenario. We use a laptop with Intel 5300 NIC WLAN card as the receiver. The laptop measures the magnitude of the WiFi Channel State Information (CSI) using Csitool [10].[4] The laptop is mounted on a Pioneer

[4]Note that the CSI magnitude captures the channel gain, which can be used as an alternative to the received signal magnitude, without affecting our framework.

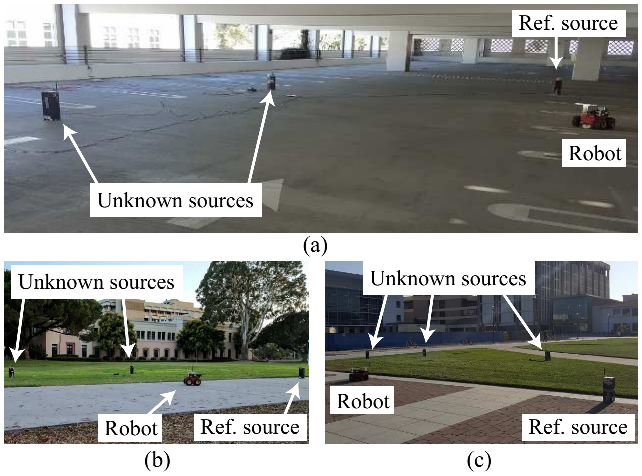

Figure 4: Experimental setup for the problem of AoA estimation of active sources in various areas on campus: (a) a closed area in a parking structure, and (b) and (c) open areas.

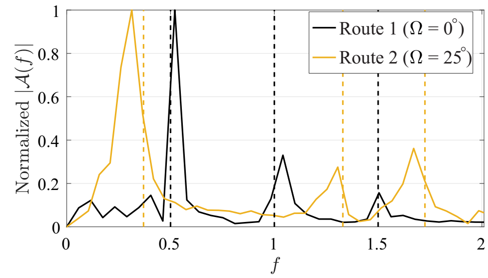

Figure 5: The normalized spectra of the auto-correlation of the magnitude measurements obtained for both routes of the robot, for the active-source AoA estimation experiment of the closed area of Fig. 4 (a). Dashed lines represent the true theoretical peak locations.

True AoAs	Estimated AoAs	
{66.42, 120}	{67.74, 120.22}	(Top) *Two arrays*
{66.42, 120}	{66.14, 120.29}	
{66.42, 120, 143.13}	{65.99, 117.4, 140.72}	
{90, 120}	{90.43, 117.57}	
MAE	1.3°	
{66.42, 120}	{68.18, 121.27}	(Bottom) *Dominant reference source & one array*
{66.42, 120}	{64.88, 117.7}	
{66.42, 120, 143.13}	{64.59, 117.3, 140.9}	
{66.42, 120, 143.13}	{68.15, 121.1, 146.2}	
{66.42, 120, 143.13}	{61.52, 117.7, 146.2}	
MAE	2.79°	

Table 1: Summary of the experimental results for AoA estimation of active sources – (top) solved with proposed approach of Sec. 3.1.2 with two robotic arrays, and (bottom) solved with the proposed approach of Sec. 3.1.3, with a dominant reference source and one robotic array.

3-AT mobile robot [11], and the robot moves along a linear route. The motion of the robot enables signal measurements at several locations along the route, thus emulating an antenna array. We utilize a spatial sampling frequency of 10 samples/cm, which is well above the Nyquist sampling rate. It should be noted that while the Intel 5300 card is capable of reporting a measurement for the phase of the signal, the phase measurement at different robot positions can not be properly related to each other due to frequency drift and other sources of random errors [33].

3.2.1 AoA Estimation of Active Sources. In this section, we present our experimental results for the AoA estimation of signals arriving from multiple active sources (transmitters) in both closed and open areas. Consider the closed area shown in Fig. 4 (a). One reference source is located at an angle $\phi_{\text{ref}} = 0°$ and 2 unknown sources are located such that their true AoAs are 90° and 120°. The robot then collects measurements along two routes of length 1 m each, with the orientations of the routes corresponding to $\Omega = 0°$ and $\Omega = 25°$. Fig. 5 then shows the normalized spectra of the auto-correlation functions $|\mathcal{A}(f)|$ across the arrays, for both routes of the robot. It can be seen that the second array configuration results in a different set of distances. We identify the peaks as those points with a minimum prominence value of 10% of the maximum peak (a point is a peak if it is higher than its neighbors by 10% of the max peak value). Then, using our proposed framework of Sec. 3.1, we obtain a unique final solution as $\{0, 90.43, 117.57\}$, resulting in a Mean Absolute Error (MAE) of 1.43°.

Additionally, we performed several other experiments in the open and closed areas of Fig. 4 (a-c) . Table 1 (top) summarizes the results of 4 different experiments carried out in these locations. We can see that our proposed framework can estimate the AoAs of multiple sources accurately, with an overall MAE of 1.3°.

3.2.2 AoA Estimation of Active Sources with a Dominant Reference Source. In the previous results, no assumptions were made regarding the power level of the active sources as compared to the reference source. Instead, two robotic routes were used to uniquely find the AoAs. As we proposed in Sec. 3.1.3, if the reference source is non-negligibly stronger than the unknown active sources, we can then solve for the unknown sources with only one robotic route and with a simpler approach. We next experimentally validate this case. A dominant reference source with a high power is located at an angle $\phi_{\text{ref}} = 0°$. For the dominant reference source, we use an antenna with a 12 dB higher gain than the antennas of the other unknown sources. Table 1 (bottom) then summarizes our results using our proposed approach of Sec. 3.1.3, for experiments in the three areas shown in Fig. 4. We can see that our proposed framework accurately estimates the AoA in this case as well, with an MAE of 2.79°.

3.2.3 AoA Estimation of Passive Objects. We next present our experimental results for the AoA estimation of passive objects. AoA estimation then refers to estimating the direction of these objects with respect to the antenna array. Consider the scenario shown in Fig. 6 (c), for instance. Our reference source is located at an angle of $\phi_{\text{ref}} = 0°$ and two humans are standing at angles $\phi_1 = 90°$ and $\phi_2 = 110°$. Since the reference source will be dominant in the passive case, we can use the framework of Sec. 3.1.3, and directly estimate the AoA, using one robotic array, and from the spectrum

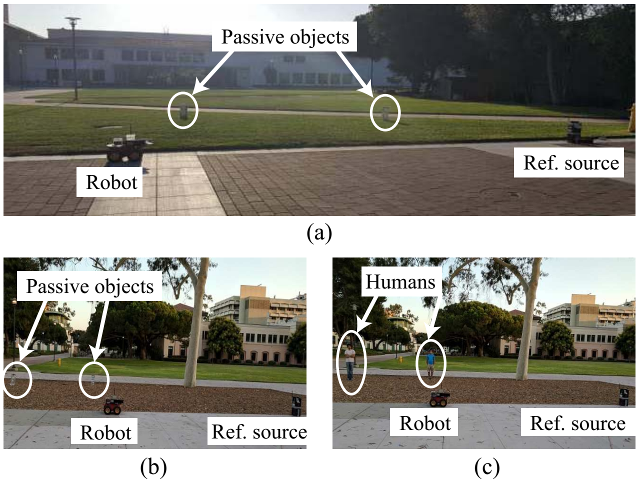

Figure 6: Experimental setup for the AoA estimation (estimation of the direction) of passive sources in various areas on our campus: (a)–(b) passive objects, and (c) humans.

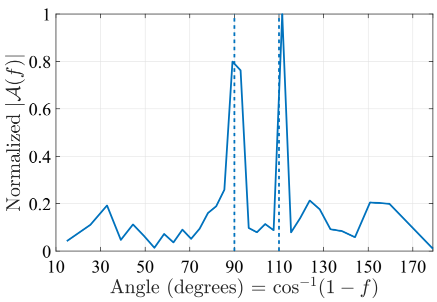

Figure 7: A sample normalized spectrum of the auto-correlation of magnitude measurements for the passive case of two humans in the area of Fig. 6 (c), using only one robotic array. Dashed lines represent the true AoAs.

True AoAs	Estimated AoAs	
{90, 120}	{92.38, 124.2}	*2 objects*
{90, 110}	{89.14, 111.4}	
{45, 90}	{42.18, 80.14}	
{45, 69, 90}	{46.68, 64.88, 86.66}	*3 objects*
{90, 110}	{89.14, 111.4}	*2 humans*
MAE	2.99°	

Table 2: Summary of the AoA experimental results (angular localization) for the case of passive objects/humans, using one robotic array.

shown in Fig. 7. As can be seen, the peaks in the spectrum are located at angles 89.14° and 111.4°, which are very close to the true angles, resulting in an MAE of 1.13°. Table 2 summarizes the results of 5 different experiments for passive objects, carried out in the three locations shown in Fig. 6. The overall MAE is 2.99° over all the passive experiments, indicating a very good accuracy.

3.2.4 Performance with Additional Phase Information. We next compare the performance of our magnitude-only approach with the case where phase can be additionally measured in the receiver. More specifically, we performed a set of 5 active-source experiments using USRP N210 Software Defined Radio (SDR) platforms [20], thus measuring both the received signal magnitude and phase. We then estimated the AoAs of signals arriving from the active sources by using the additional phase information and traditional beamforming. The resulting MAE of AoA estimation when additional phase information was available was 0.93°. On the other hand, the corresponding MAE, using our proposed AoA estimation framework and with only magnitude measurements, was 1.76°. This shows that our proposed approach that uses only signal magnitude has a performance comparable to the case where additional phase information is available.

Overall, our proposed framework can accurately estimate the AoA of fixed active sources as well as passive objects, using only magnitude of the received signal measurements. *Our approach is also computationally efficient.* For instance, it took an average of 0.45 seconds (averaged over all the 14 presented results) to find the final solution in MATLAB.

Next, we show how our AoA estimation framework can be adapted to track a moving target (both active and passive).

4 TRACKING A MOVING TARGET

In this section, we show how our proposed magnitude-only AoA estimation approach can be deployed to track a moving active or passive target, using only the magnitude of the received signal at a small number of receivers. By an active moving target, we mean a moving transmitter, such as a moving vehicle that emits a signal as it moves. A passive target, on the other hand, refers to a moving object that has no transmitter on board, such as a moving human or robot that does not emit any signal. We first show the duality between the target tracking problem and the previous AoA estimation problem of fixed sources. Then, we show that using the aforementioned methodology, in conjunction with motion dynamics, can localize and track a moving target. We start by discussing the active target tracking scenario.

Active Target Tracking: Consider the scenario shown in Fig. 8 (a), where a known fixed receiver (Rx) receives wireless signals from a known fixed transmitter ($\mathrm{Tx}_{\mathrm{fix}}$) and an unknown moving active transmitter ($\mathrm{Tx}_{\mathrm{mov}}$). $\mathrm{Tx}_{\mathrm{mov}}$ moves with a constant speed, v, along a line that makes an angle $\theta_\circ$ with the x-axis, and an angle ϕ_r with the line connecting $\mathrm{Tx}_{\mathrm{mov}}$ and Rx, as shown in the figure. The total baseband received signal at the receiver at time t, $c(t)$, will then be,

$$c(t) = \alpha_1 e^{j\mu_1} + \alpha_2 e^{j(\mu_2 - \frac{2\pi}{\lambda} v\psi_r t)} + \eta(t), \tag{4}$$

where α_1, α_2 are the amplitudes of the paths from $\mathrm{Tx}_{\mathrm{fix}}$ and $\mathrm{Tx}_{\mathrm{mov}}$, respectively. Parameter μ_1 is the phase of the signal arriving from $\mathrm{Tx}_{\mathrm{fix}}$, μ_2 is the phase of the signal from $\mathrm{Tx}_{\mathrm{mov}}$ when the moving target is at its initial position ($t = 0$), v is the speed of $\mathrm{Tx}_{\mathrm{mov}}$, and $\psi_r = \cos(\phi_r)$. By comparing Eq. 4 and Eq. 1, we can see the equivalence between the two equations, where Eq. 4 can be considered a special case of Eq. 1 with $N = 2$ sources, $\psi_1 = 0$ and $\psi_2 = \psi_r$. Basically, the magnitude-only tracking problem can be considered as the *dual* of our previous AoA estimation problem, where the moving transmitter $\mathrm{Tx}_{\mathrm{mov}}$ synthesizes a transmit array, and the

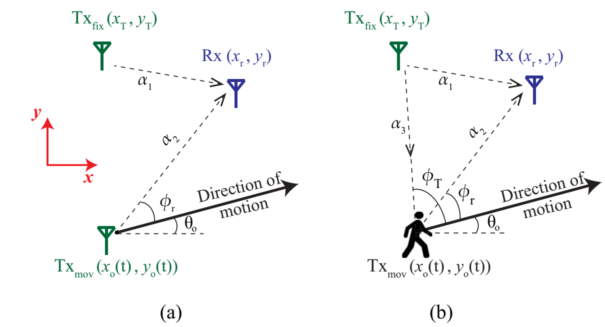

Figure 8: The setup for tracking a moving (a) active target, and (b) passive target, with only magnitude measurements at the receiver.

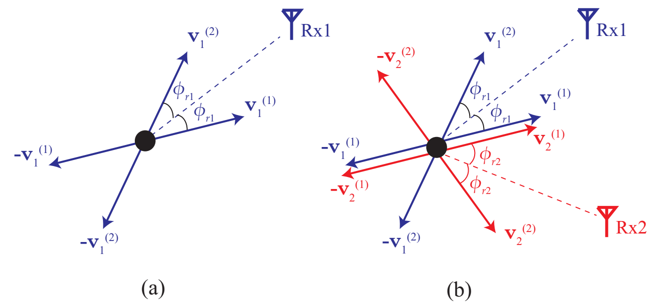

Figure 9: An example of bearing estimation ambiguity for active tracking – (a) Using one Rx, four different velocity vectors ($\pm\mathbf{v}_1^{(1)}$ and $\pm\mathbf{v}_1^{(2)}$) result in the same measurement of $|\cos(\phi_{r_1})|$ at Rx1. (b) Using two Rx, only two velocity vectors ($\pm\mathbf{v}_1^{(1)}$) result in measuring $|\cos(\phi_{r_1})|$ and $|\cos(\phi_{r_2})|$ at Rx1 and Rx2 simultaneously.

quantity ψ_r relates to the angle of departure instead of the AoA. Therefore, we can use our framework of Sec. 2 to estimate $|\psi_r|$.

Remark 5. *Note that if there are unknown fixed transmitters in the area, they will not affect the tracking quality. This is due to the fact that any fixed transmitter will result in a constant term (such as the first term in Eq. 4) with $\psi = 0$. Thus, the non-DC peaks of the spectrum will only correspond to ψ_r. This is in particular attractive as the signal may bounce of other fixed objects in the area, creating several paths to the receiver.*

Passive Target Tracking: Consider the case where we are interested in tracking an unknown moving target that is passive, i.e. the target does not have a signal source onboard, but reflects the incident signal from Tx_{fix}, as shown in Fig. 8 (b). The received signal at Rx can then be written as follows:

$$c(t) = \alpha_1 e^{j\mu_1} + \gamma\alpha_2\alpha_3 e^{j(\mu_2 - \frac{2\pi}{\lambda} v\psi_r t)} + \eta(t), \tag{5}$$

where the first term is the same as the first term in Eq. 4, γ is the reflection coefficient from the moving target, μ_2 is the phase of the reflected path when the target is at its initial position ($t = 0$), and $\psi_r = \cos(\phi_r) + \cos(\phi_T)$. Similar to the active case, the duality between Eq. 5 and Eq. 1 can be seen. Thus, we can use our framework of Sec. 2 to estimate $|\psi_r|$, which, in this case, is equal to $|\cos(\phi_r) + \cos(\phi_T)|$.

Resolving the Tracking Ambiguity: In general, our magnitude-based tracking problem is easier than our previous AoA estimation of fixed sources since there is only one angle to be estimated per moving target, and the impact of all non-moving transmitters/objects will not be seen in the power spectrum. However, there are still ambiguities if only one receiver is used, as we shall explain next. Our tracking problem consists of estimating the location and bearing of Tx_{mov} at each time instant t. However, using $|\psi_r|$ as the only piece of information would result in ambiguities when solving such a problem. For instance, consider the problem of using one receiver to estimate the bearing of the active target, as shown in Fig. 9 (a). The target has a velocity vector $\mathbf{v}_1^{(1)}$. It moves in a direction that makes an angle ϕ_{r_1} with the line connecting the target and the receiver Rx1. This results in $|\psi_{r_1}| = |\cos(\phi_{r_1})|$ at the receiver Rx1. Then, as shown in Fig. 9 (a), four different velocity vectors ($\pm\mathbf{v}_1^{(1)}$ and $\pm\mathbf{v}_1^{(2)}$) can result in the same measurement. Thus, Rx1 cannot uniquely estimate the true bearing of the moving target. In addition, the starting point of the target can be any point in the workspace, adding more ambiguity to the solution. To solve the bearing ambiguity, we can add more receivers. For instance, by adding one more receiver, we can see that two of those four solutions of Fig. 9 (a) will become invalid, as shown in Fig. 9 (b). However, there will still be the ambiguity between the actual velocity vector and the one pointing to the opposite direction. Adding more receivers will not resolve this specific type of ambiguity. It is easy to confirm that the passive case will also have ambiguities.

Since the main goal of this section is to track a moving target (active or passive), including its location and bearing, we use a small number of receivers to reduce the aforementioned bearing ambiguity. We furthermore utilize a non-linear dynamical system to represent the motion dynamics of the target. This dynamical system modeling, in conjunction with the receiver measurements, will then remove the remaining ambiguity of the bearing, as well as the location ambiguity, as we shall see next.

4.1 Nonlinear Dynamical System Modeling

Consider the scenario where there are a total of R receivers located at (x_{r_i}, y_{r_i}), $1 \le i \le R$, a fixed transmitter Tx_{fix} located at (x_T, y_T), and a moving target Tx_{mov} located at $(x_\circ(t), y_\circ(t))$ at time t. The *state* of the target at time t is defined as the 3-dimensional vector $\mathbf{x}_t = [x_\circ(t), y_\circ(t), \theta_\circ(t)]^T$, where $\theta_\circ(t)$ is the bearing of Tx_{mov} at time t, and $[.]^T$ is the transposition operator. A measurement process $\mathbf{\Psi}_t$ is an R-dimensional vector of measurements from all the receivers: $\mathbf{\Psi}_t = [|\hat{\psi}_{r_1}(t)|, |\hat{\psi}_{r_2}(t)|, \ldots, |\hat{\psi}_{r_R}(t)|]^T$, where $|\hat{\psi}_{r_i}(t)|$ is the measurement obtained at the i^{th} receiver at time t. In case of an active target, this measurement is related to the state of the target as follows:

$$|\hat{\psi}_{r_i}(t, \mathbf{x}_t)| = \left| \frac{(x_{r_i} - x_\circ(t))\, cos\,(\theta_\circ(t)) + (y_{r_i} - y_\circ(t))\, sin\,(\theta_\circ(t))}{\sqrt{(x_{r_i} - x_\circ(t))^2 + (y_{r_i} - y_\circ(t))^2}} \right| + w_{r_i}(t), \tag{6}$$

where $w_{r_i}(t)$ is the Gaussian measurement noise at receiver r_i, with variance $\sigma_{w_r}^2$. On the other hand, in the case of passive target, $\mathbf{\Psi}_t$

is related to the state of the target as,

$$|\hat{\psi}_{r_i}(t, \mathbf{x}_t)| = \left| \frac{\big(x_{r_i} - x_\circ(t)\big)\, cos\,(\theta_\circ(t)) + \big(y_{r_i} - y_\circ(t)\big)\, sin\,(\theta_\circ(t))}{\sqrt{(x_{r_i} - x_\circ(t))^2 + (y_{r_i} - y_\circ(t))^2}} + \frac{(x_T - x_\circ(t))\, cos\,(\theta_\circ(t)) + (y_T - y_\circ(t))\, sin\,(\theta_\circ(t))}{\sqrt{(x_T - x_\circ(t))^2 + (y_T - y_\circ(t))^2}} \right| + w_{r_i}(t). \tag{7}$$

For the dynamics of $\mathbf{x}_t$, we adopt a simple constant-speed motion model, $\mathbf{x}_{t+1} = g(\mathbf{x}_t)$, as follows:

$$\begin{aligned} x_\circ(t+1) &= x_\circ(t) + v\ \cos(\theta_\circ(t)) + w_{x_\circ}(t+1), \\ y_\circ(t+1) &= y_\circ(t) + v\ \sin(\theta_\circ(t)) + w_{y_\circ}(t+1), \\ \theta_\circ(t+1) &= w_{\theta_\circ}(t+1) + \begin{cases} \theta_\circ(t) & \text{w.p. } P_c \\ \sim \mathcal{U}(0, 2\pi) & \text{w.p. } 1 - P_c, \end{cases} \end{aligned} \tag{8}$$

where $w_{x_\circ}, w_{y_\circ}, w_{\theta_\circ}$ are the noise processes for the three components of the target state $x_\circ$, $y_\circ$, and $\theta_\circ$, respectively, and P_c is the probability of the target maintaining the same bearing as the previous time instant. Eq. 8 along with Eq. 6, or Eq. 7, then defines the nonlinear dynamical system of the tracking problem.

To estimate the state of the moving target, we compute the conditional probability of the target having a state $\mathbf{x}_t$ given all the measurements up to time t, $p(\mathbf{x}_t|\mathbf{\Psi}_{1:t})$. In the filtering literature, this probability is referred to as the *filtering Probability Density Function (PDF)*. Then, we use the mean of this PDF, $E\{\mathbf{x}_t|\mathbf{\Psi}_{1:t}\}$, as the estimate for the target state at time t. Since the dynamical system is nonlinear, we utilize particle filtering to compute the filtering PDF [25]. We next briefly discuss the particle filtering algorithm. In a Particle Filter (PF), a probability distribution is represented by a set of random samples, called *particles*, drawn from that distribution. Such a representation is desirable because it can easily model nonlinear transformations of random variables, which makes it particularly suitable for the problem at hand. The basic idea of a PF is that, at each time instant, samples (or *particles*) are drawn from a proposal distribution $\mathbf{x}_t^{[i]} \sim \zeta_t(\mathbf{x}_t)$, $i = 1, \ldots, I$, where I is the total number of particles. Those particles are then given *importance weights*, $w_t^{[i]}$, that describe how well they fit the current measurement $\mathbf{\Psi}_t$. That set of weighted particles represent the filtering PDF $p(\mathbf{x}_t|\mathbf{\Psi}_{1:t})$ at time t. Afterwards, a *resampling* step is performed. This step is crucial in order to neglect particles with very low weights (very low probability of producing the current measurement) and focus more on particles with high weights. Specifically, a new set of I particles are drawn from the distribution defined by $w_t^{[i]}$ over the values of $\mathbf{x}_t^{[i]}$. The readers are referred to [25] and [27] for more on PF.

The PF for our framework is described in Algorithm 2. In step 2, we draw the particles of the initial state from an initial distribution $\zeta_1(\mathbf{x}_1)$, which can depend on any prior information we may have about the initial state of the target (or is taken to be uniform when no prior information is available). Then, step 3 calculates the importance weight of each particle as the probability of getting the measurement $\mathbf{\Psi}_1$, given that the state of the target is this particle. This probability can be easily calculated using the measurement model in Eq. 6 or 7 (depending on whether an active or passive target is being tracked). Step 6 is the resampling step, which is important for discarding low weight particles, as mentioned before. Step 7 is where the motion dynamics are enforced into the tracking problem. The resampled particles are evolved according to the motion model in Eq. 8. This is a very simple and intuitive way of producing the proposal density of particles of the next time instant. After the tracking period T is over, the estimated track of the object $E\{\mathbf{x}_t|\mathbf{\Psi}_{1:t}\}\,|_{t=1:T}$ is smoothed by passing it through a spatial moving average filter.

Algorithm 2 Particle filter for motion tracking

Input: Total tracking time T, Number of particles I, Measurements $\mathbf{\Psi}_{1:T}$
Output: Estimate of the target states $\hat{\mathbf{x}}_{1:T}$.

1: Initialize $t = 1$
2: Sample $\mathbf{x}_1^{[i]} \sim \zeta_1(\mathbf{x}_1)$ for $i = 1, 2, \ldots, I$
3: Compute the importance weights $\tilde{w}_1^{[i]} = p(\mathbf{\Psi}_1|\mathbf{x}_1 = \mathbf{x}_1^{[i]})$ and normalize $w_1^{[i]} = \frac{\tilde{w}_1^{[i]}}{\sum_{i=1}^{I} \tilde{\mathrm{w}}_1^{[i]}}$
4: Estimate the initial target state $\hat{\mathbf{x}}_1 = E\{\mathbf{x}_1|\mathbf{\Psi}_1\} = \sum_{i=1}^{I} w_1^{[i]}\mathbf{x}_1^{[i]}$
5: **for** $2 \le t \le T$ **do**
6: Sample $\tilde{\mathbf{x}}_{t-1}^{[i]}$, for $i = 1, \ldots, I$, from the distribution defined by $p(\tilde{\mathbf{x}}_{t-1} = \mathbf{x}_{t-1}^{[i]}) = w_{t-1}^{[i]}$.
7: Sample $\mathbf{x}_t^{[i]} \sim g(\tilde{\mathbf{x}}_{t-1}^{[i]})$
8: Compute the importance weights $\tilde{w}_t^{[i]} = p(\mathbf{\Psi}_t|\mathbf{x}_t = \mathbf{x}_t^{[i]})$ and normalize $w_t^{[i]} = \frac{\tilde{w}_t^{[i]}}{\sum_{i=1}^{I} \tilde{\mathrm{w}}_t^{[i]}}$
9: Estimate the target state $\hat{\mathbf{x}}_t = \sum_{i=1}^{I} w_t^{[i]}\mathbf{x}_t^{[i]}$
10: **end for**

4.2 Tracking Experimental Results

In this section, we present experimental results for our proposed framework for target tracking, using only the received signal magnitude at the receiver. We use a similar setup to the one in Sec. 3.2, for transmission and reception, with three laptops as receivers. The router operates in the WiFi 5GHz band. All laptops are equipped with Intel 5300 NIC WLAN card and use Csitool to measure the WiFi CSI [10]. Since the target is moving and can change its direction anytime, we use the framework of Sec. 2 on a moving time window, T_{win}, of the CSI magnitude time series. More specifically, for each window, we extract $|\psi_r|$ from the location of the peak of the spectrum of the received signal magnitude auto-correlation within this window. These measurements are then aggregated and processed offline to estimate the track of the target (see Remark 6 on online tracking). Note that the receivers are not time-synchronized and operate independently, where each receiver logs CSI from packets that are broadcast on the network. We achieve this by using iPerf tool [12] to broadcast packets from the transmitter. We next discuss practical considerations that arise in the experiments before presenting our results.

4.2.1 *Practical Considerations.*

- Window Length: As a compromise between having a larger T_{win} for better frequency resolution (i.e., longer array length), and a

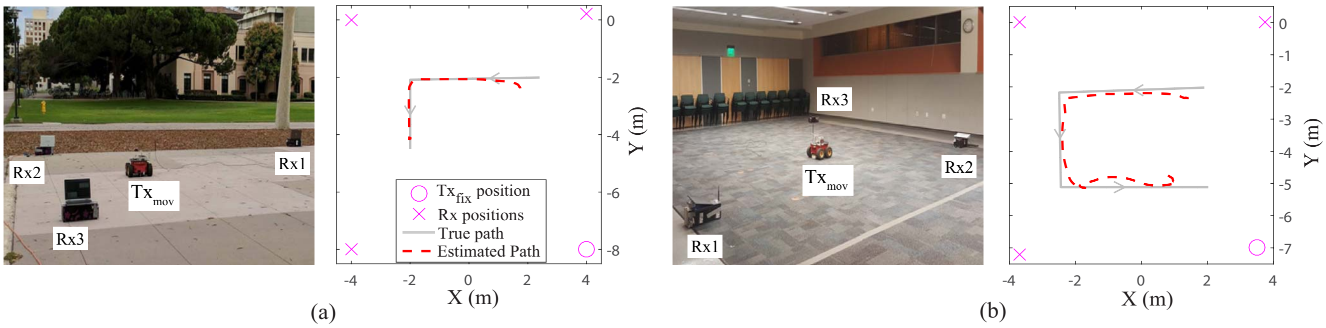

Figure 10: (a) (left) A robot with an active transmitter Tx_{mov} is being tracked by 3 receivers in an open area, and (a) (right) an accurate reconstruction of the tracking route using our proposed framework. (b) (left) A robot with an active transmitter is being tracked by three receivers in a closed area, and (b) (right) an accurate reconstruction of the tracking route using our proposed framework.

smaller T_{win} for shorter distance traveled by the target (resulting in a better piece-wise linear approximation of the route), we set $T_{\text{win}} = 1/v$ corresponding to 1 m of distance moved by the object.

- Subcarrier Selection: The spectrum of each window should theoretically include one Dirac delta function whose frequency is $|\psi_r|$. However, transmission in some subcarriers may be less informative due to more noise and interference. Therefore, we use the variance of the power distribution in the frequency spectrum (after DC removal), as an indication of the clarity of the subcarrier data, for each time window. The subcarrier with the minimum average variance across all time windows is chosen for extracting $|\psi_r|$.
- Frequency Resolution: Since a receiver calculates the spectrum using only a windowed time signal, the frequency bins of the FFT spectrum in Eq. 3 are spaced $\lambda/(vT_{\text{win}})$ apart, and the peak of the spectrum will be detected at the bin closest to the true peak. This adds a *quantization* effect to the time series of the measured $|\hat{\psi}_r|$. Therefore, we first pass the measured $|\hat{\psi}_r(t)|$ through a moving average filter of length T_{win} to reduce the quantization effect, prior to using it in the PF. It should be noted that sudden rapid changes in the time series of $|\hat{\psi}_r|$ at more than one receiver at the same time, could be an indication of motion direction change. When such a change is detected, the moving average filters are re-initialized so that different segments of the route are filtered separately.
- PF Parameters: We set the parameters of the PF as follows: $I = 8000$, $P_c = 0.9$, $\sigma_{w_r} = 0.1$, $\sigma_{w_{x_o}} = \sigma_{w_{y_o}} = 1$ cm, and $\sigma_{w_{\theta_o}} = 1°$. The values of the noise variances were estimated by measuring the errors in the robot motion and in the $|\psi_r|$ measurements of prior experiments (not in the same area), and fitting Gaussian distributions to the respective measurement errors. After the PF, the moving average filter has a spatial width of 0.5 m.

4.2.2 Tracking an Active Moving Target. In this section, we show experimental results for tracking an active moving transmitter in both a closed and an open area. For the open area, consider the setup shown in Fig. 10 (a) (left), where three receivers are located at the corners of an 8 m × 8 m area, and are tasked with tracking a moving robot with an active transmitter. The robot moves in an L-shaped route with a constant speed of $v = 0.1$ m/s. The PF was initialized with particles uniformly distributed in a 4 m × 4 m

Figure 11: Passive robot tracking experimental setup in (left) a closed area and (right) an open area.

square area in the upper right quadrant of the area. Fig. 10 (a) (right) shows the tracking result of this case, which demonstrates a highly accurate reconstruction of the robot path, with a tracking mean absolute error (MAE) of 11.3 cm. For the closed area shown in Fig. 10 (b) (left), the same setting is used inside a room to track an active transmitter robot that moves in a U-shaped route in a 7 m × 7 m area. It can be seen from the tracking result of Fig. 10 (b) (right) that our framework tracks the robot accurately indoors, with an MAE of 30.6 cm.

4.2.3 Tracking a Passive Moving Target. We next show how our approach can track passive moving targets. We consider two scenarios: (a) tracking a passive moving object, and (b) tracking a walking human. For the passive moving object, we track a non-transmitting robot that moves in both an 8 m × 8 m open area and an 8 m × 8 m closed area, as shown in Fig. 11. The routes of the robot are designed such that they spell the letters of the word *IPSN*, with the letters I and P in the closed area, and the letters S and N in the open area. In all the experiments, we initialize the PF uniformly over a 4 m × 4 m area around the area that the robot starts. Fig. 12 shows the results of the tracking experiments. It can be seen that we can track the passive robot well in all the cases, with an MAE of 23.27 cm. It should be noted that the dimensions of the robot are 50 cm × 40 cm, and the signal might bounce off of any part of the robot's outer frame. This is in contrary to the active tracking case where the location of the transmitter is clear. Thus, we calculate the error in this case as the minimum distance between the estimated position and the robot frame at each time step.

For the human tracking experiment, a person was asked to walk in an 8 m × 8 m area as shown in Fig. 13 (left). Since the average

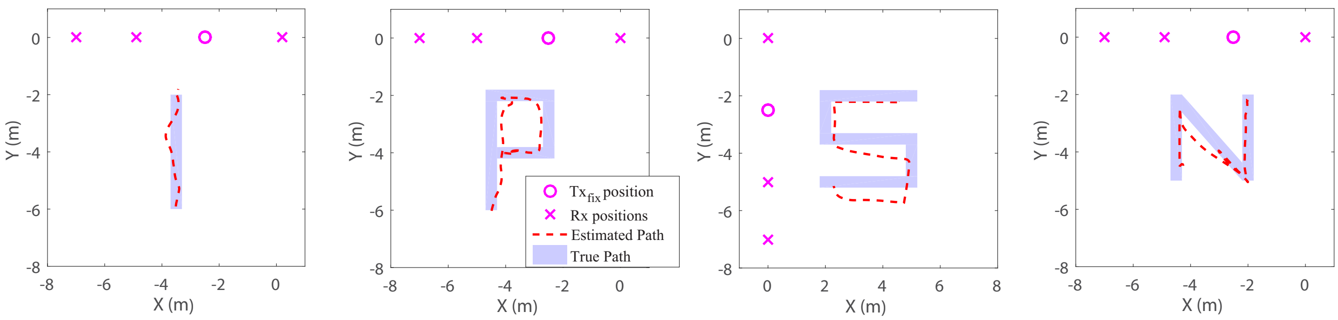

Figure 12: Passive robot tracking results for a robot that writes the letters of *IPSN* on its route, in the two areas of Fig. 11. The letters I and P were tracked in the closed area of Fig. 11 (left), while the letters S and N were tracked in the open area of Fig. 11 (right).

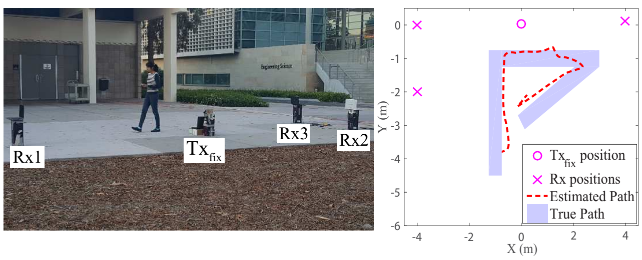

Figure 13: (left) The experimental setup for the passive human tracking scenario and (right) the estimated route of the human using our proposed framework.

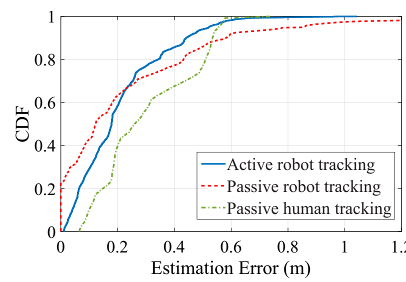

Figure 14: CDFs of the tracking error of our framework for active transmitter tracking, passive robot tracking and passive human tracking. Our proposed framework achieves a decimeter-level accuracy for all the different scenarios.

human speed (assumed to be 0.8 m/s) is higher than the robot speed, we use a laptop for the fixed transmitter, instead of a router, in order to have a higher sampling rate. Since the human body is not a strong reflector, we use the 2.4 GHz band for the human experiments in order to have a smaller path loss attenuation. Fig. 13 (right) shows the human tracking result. It can be seen that our proposed framework accurately tracks the person's complicated route, with an MAE of 30.26 cm. Similar to the passive robot tracking case, we do not know the exact location where the signal might have bounced off of the human body. Thus, by assuming the human to be a cylinder of radius 20 cm, we calculate the error as the minimum distance between the estimated position and the edge of the cylinder at each time step.

Fig. 14 shows the Cumulative Distribution Function (CDF) curves of the absolute tracking estimation error, for both the active and passive cases. It can be seen that our proposed framework achieves a good tracking quality, with only WiFi magnitude measurements at 3 receivers (i.e., 3 links).

Our proposed framework of tracking using a PF is very efficient and of very low computational complexity. More specifically, the average run-time per 1 m of tracking length is 1.05 sec, over all the experiments. This is in contrast to the state-of-the-art tracking systems [17, 22], which use 6 links to achieve comparable tracking accuracy (38 cm MAE in [22] and 35 cm median error in [17]), and where high computational complexity has been reported.

Remark 6 (on Data Aggregation Latency). *For a real-time implementation, a central processor needs to aggregate measurements from the 3 receivers, in order to process them and track the moving target online. According to the state-of-the-art [2], such a process takes about 9 ms to aggregate the data of the three receivers. Thus, the required time for the data aggregation is less than the required channel sampling time at the receivers ($\frac{\lambda}{4v}$), allowing the central processor to aggregate the data from all the receivers before the next channel sampling instant. Hence, the data aggregation process does not add any latency to the system.*

5 LIMITATIONS AND FUTURE EXTENSIONS

In this paper, we have proposed an approach that has enabled AoA estimation and target tracking using only the magnitude of the wireless signals, which is an extremely challenging problem. Here are some possible directions to further extend this work:

- **Validation in more complex environments:** In this paper, we validated our framework with several experiments in Line-of sight (LOS) settings, in both open and closed areas. However, more complex spaces can result in a non line-of-sight (NLOS) operation, to which our framework is extendable. A more detailed analysis and testing of the proposed methods in through-wall settings is part of our future work. As for multipath, more complex environments can also experience a high level of multipath. As mentioned in Remark 5, and showcased by our results in closed spaces, multipath does not affect our tracking framework. As part of our future work, we plan to test our framework in more indoor spaces that can experience a high level of multipath.
- **Multiple target tracking:** Our proposed tracking framework has enabled tracking of a single moving target, even in the presence of other static targets in the area. For the case of multiple moving targets, more than one peak will appear in the frequency

spectrum. As part of our future work, we can extend the tracking framework to simultaneously track a number of moving targets.

6 CONCLUSIONS

In this paper, we have considered the problem of estimating the angle of arrival (AoA) of all signal paths arriving at a receiver array using only the received signal magnitude measurements. We have proposed a computationally-efficient framework, based on the auto-correlation of the magnitude measurements, to solve the AoA estimation problem. We have experimentally validated our AoA estimation framework in closed and open areas, and showed a mean absolute error of 2.12° for the active source case, and 2.99° for passive objects. Furthermore, we have adapted the magnitude-based AoA estimation approach to track an active/passive moving target. Our tracking framework was experimentally validated in various closed and open areas, with only three receivers, and showed good tracking accuracy, with an overall MAE of 20 cm for active target tracking, 23.27 cm for passive robot tracking, and 30.62 cm for passive human tracking.

ACKNOWLEDGMENTS

The authors would like to thank the anonymous reviewers and the shepherd for their valuable comments and helpful suggestions. This work is funded by NSF CCSS award # 1611254.

A MAGNITUDE AUTO-CORRELATION

Let $c_I(d)$ and $c_Q(d)$ be the real and imaginary parts of $c(d)$. The auto-correlation function of $c_I(d)$ can be written as

$$A_I(\Delta) = E\{c_I(d)c_I(d+\Delta)\} = \sum_{n=1}^{N} \frac{\overline{\alpha_n^2}}{2} \cos\left(2\pi\frac{\Delta}{\lambda}\psi_n\right) + \frac{1}{2}\sigma_\eta^2\delta(\Delta),$$

where $\psi_n = \cos(\phi_n)$, σ_η^2 is the variance of noise, and $\delta(.)$ is the Dirac delta function. In a similar fashion, the cross-correlation between $c_I(d)$ and $c_Q(d)$ can be written as

$$A_{I,Q}(\Delta) = E\{c_I(d)c_Q(d+\Delta)\} = \sum_{n=1}^{N} \frac{\overline{\alpha_n^2}}{2} \sin\left(2\pi\frac{\Delta}{\lambda}\psi_n\right).$$

Define $\rho^2(\Delta) = \frac{1}{P^2}\left(A_I^2(\Delta) + A_{I,Q}^2(\Delta)\right)$, where P is the total received power, then [13]

$$\begin{aligned}
A_{\text{corr}}(\Delta) &= \frac{\pi P}{2}\left(1 + \frac{\rho^2(\Delta)}{4} + \frac{\rho^4(\Delta)}{64} + \dots\right) \approx \frac{\pi P}{2}\left(1 + \frac{\rho^2(\Delta)}{4}\right) \\
&= \frac{\pi}{2}P + \frac{\pi}{8P}\left(A_I(\Delta) + jA_{I,Q}(\Delta)\right)\left(A_I(\Delta) - jA_{I,Q}(\Delta)\right) \\
&= C_A + C_{\sigma_\eta}\delta(\Delta) \\
&\quad + \frac{\pi}{16P}\sum_{n=1}^{N}\sum_{m>n} \overline{\alpha_n^2\alpha_m^2}\cos\left(2\pi\frac{\Delta}{\lambda}(\psi_n - \psi_m)\right).
\end{aligned}$$

REFERENCES

[1] F. Adib and D. Katabi. 2013. See Through Walls with WiFi!. In *Proc. of the ACM SIGCOMM 2013 Conference.* 75–86.

[2] M. Bocca, O. Kaltiokallio, and N. Patwari. 2012. Radio tomographic imaging for ambient assisted living. In *International Competition on Evaluating AAL Systems through Competitive Benchmarking*. Springer, 108–130.

[3] M. Bocca, O. Kaltiokallio, N. Patwari, and S. Venkatasubramanian. 2014. Multiple target tracking with RF sensor networks. *IEEE Trans. on Mobile Computing* 13, 8 (2014), 1787–1800.

[4] S. Chang, R. Sharan, M. Wolf, N. Mitsumoto, and J. Burdick. 2009. UWB radar-based human target tracking. In *IEEE Radar Conference, 2009.*

[5] Y. Chen, D. Lymberopoulos, J. Liu, and B. Priyantha. 2012. FM-based indoor localization. In *Proc. of the 10th ACM International Conf. on Mobile Systems, Applications, and Services.*

[6] S. Depatla, L. Buckland, and Y. Mostofi. 2015. X-ray vision with only WiFi power measurements using rytov wave models. *IEEE Trans. on Vehicular Technology* 64, 4 (2015), 1376–1387.

[7] S. Depatla, A. Muralidharan, and Y. Mostofi. 2015. Occupancy estimation using only WiFi power measurements. *IEEE J. on Selected Areas in Communications* 33, 7 (2015), 1381–1393.

[8] A. Gonzalez-Ruiz, A. Ghaffarkhah, and Y. Mostofi. 2014. An integrated framework for obstacle mapping with see-through capabilities using laser and wireless channel measurements. *IEEE Sensors J.* 14, 1 (2014).

[9] A. Gonzalez-Ruiz and Y. Mostofi. 2013. Cooperative robotic structure mapping using wireless measurements- a comparison of random and coordinated sampling patterns. *IEEE Sensors J.* 13, 7 (2013), 2571–2580.

[10] D. Halperin, W. Hu, A. Sheth, and D. Wetherall. 2011. Tool release: Gathering 802.11n traces with channel state information. *ACM SIGCOMM CCR* 41, 1 (Jan. 2011), 53.

[11] Mobile Robots Inc. 2010. Pioneer 3-AT. (2010). http://www.mobilerobots.com

[12] IPERF. 2017. iPerf Network Measurement Tool. (2017). https://iperf.fr/

[13] W. C. Jakes and D. C. Cox. 1994. *Microwave mobile communications.* Wiley-IEEE Press.

[14] C. R. Karanam and Y. Mostofi. 2017. 3D through-wall imaging with unmanned aerial vehicles using WiFi. In *Proc. of the 16th ACM/IEEE International Conf. on Information Processing in Sensor Networks.*

[15] H. Kim, A. M. Haimovich, and Y. C. Eldar. 2015. Non-coherent direction of arrival estimation from magnitude-only measurements. *IEEE Signal Processing Letters* 22, 7 (2015), 925–929.

[16] P. Lemke, S. Skiena, and W. Smith. 2003. Reconstructing sets from interpoint distances. In *Discrete and Computational Geometry.* Springer, 597–631.

[17] X. Li, D. Zhang, Q. Lv, J. Xiong, S. Li, Y. Zhang, and H. Mei. 2017. IndoTrack: Device-free indoor human tracking with commodity Wi-Fi. *Proc. ACM Interact. Mob. Wearable Ubiquitous Technol.* 1, 3 (2017), 72.

[18] J. P. Lie, T. Blu, and C. M. S. See. 2010. Single antenna power measurements based direction finding. *IEEE Trans. on Signal Processing* 58, 11 (2010), 5682–5692.

[19] G. Mao, B. Fidan, and B. Anderson. 2007. Wireless sensor network localization techniques. *Computer Networks* 51, 10 (2007), 2529–2553.

[20] USRP N210. 2015. Ettus Research. (2015). http://www.ettus.com

[21] R. Pöhlmann, S. Zhang, T. Jost, and A. Dammann. 2017. Power-based direction-of-arrival estimation using a single multi-mode antenna. *arXiv preprint arXiv:1706.09690* (2017).

[22] K. Qian, C. Wu, Z. Yang, Y. Liu, and K. Jamieson. 2017. Widar: Decimeter-level passive tracking via velocity monitoring with commodity Wi-Fi. In *Proc. of the 18th ACM International Symposium on Mobile Ad Hoc Networking and Computing.*

[23] R. Roy and T. Kailath. 1989. ESPRIT-estimation of signal parameters via rotational invariance techniques. *IEEE Trans. on Acoustics, Speech, and Signal Processing* 37, 7 (1989), 984–995.

[24] R. Schmidt. 1986. Multiple emitter location and signal parameter estimation. *IEEE Trans. on Antennas & Propagation* 34 (1986), 276–280.

[25] T. B. Schön. 2015. Nonlinear system identification using particle filters. *Encyclopedia of Systems and Control* (2015), 882–890.

[26] X. Shen, R. Fan, Q. Wan, and W. Yang. 2013. An angle difference of directions arrival algorithm with channel inconsistency. *International J. of Electronics* 100, 3 (2013), 312–318.

[27] S. Thrun, W. Burgard, and D. Fox. 2005. *Probabilistic robotics.* MIT Press.

[28] B. D. Van Veen and K. M. Buckley. 1988. Beamforming: A versatile approach to spatial filtering. *IEEE ASSP magazine* 5, 2 (1988), 4–24.

[29] H. Wang, D. Zhang, K. Niu, Q. Lv, Y. Liu, D. Wu, R. Gao, and B. Xie. 2017. MFDL: A multicarrier fresnel penetration model based device-free localization system leveraging commodity Wi-Fi cards. *arXiv preprint arXiv:1707.07514* (2017).

[30] W. Wang, A. X Liu, M. Shahzad, K. Ling, and S. Lu. 2015. Understanding and modeling of WiFi signal based human activity recognition. In *Proc. of the International Conf. on Mobile Computing and Networking.*

[31] K. Wu, J. Xiao, Y. Yi, D. Chen, X. Luo, and L. M. Ni. 2013. CSI-based indoor localization. *IEEE Trans. on Parallel and Distributed Systems* 24, 7 (2013), 1300–1309.

[32] J. Xiong and K. Jamieson. 2013. ArrayTrack: A Fine-grained Indoor Location System. In *Proc. of the 10th USENIX Conf. on Networked Systems Design and Implementation.*

[33] Y. Zhuo, H. Zhu, and H. Xue. 2016. Identifying a new non-linear CSI phase measurement error with commodity WiFi devices. In *IEEE 22nd International Conf. on Parallel and Distributed Systems (ICPADS).*